



Implications of surface flooding on airborne thickness measurements of snow on sea ice

Anja Rösel^{1,6*}, Sinead Louise Farrell², Vishnu Nandan³, Jaqueline Richter-Menge⁴, Gunnar Spreen^{5,1}, Dmitry V. Divine¹, Jean-Charles Gallet¹, and Sebastian Gerland¹

5 ¹Norwegian Polar Institute, Fram Centre, Tromsø, Norway

²Department of Geographical Sciences, University of Maryland, College Park, MD, USA

³Centre for Earth Observation Science (CEOS), University of Manitoba, MB, Canada

⁴University of Alaska Fairbanks, Fairbanks, AK, USA

⁵Institute of Environmental Physics, University of Bremen, Bremen, Germany

10 ⁶ now at Remote Sensing Technology Institute, German Aerospace Center (DLR), Wessling, Germany

*Correspondence to: Anja Rösel (anja.roesel@dlr.de)

Abstract. Snow thickness observations from airborne snow radars, such as the NASA's Operation IceBridge (OIB) mission, have recently been used in altimeter-derived sea ice thickness estimates, as well as for model parameterization. A number of validation studies comparing airborne and in situ snow thickness measurements have been conducted in the western Arctic Ocean, demonstrating the utility of the airborne data. However, there have been no validation studies in the Atlantic sector of the Arctic. Recent observations in this region suggest a significant and predominant shift towards a *snow-ice* regime, caused by deep snow on thin sea ice. During the Norwegian young sea ICE expedition (N-ICE2015) in the area north of Svalbard, a validation study was conducted on March 19, 2015, during which ground truth data were collected during an OIB overflight. Snow and ice thickness measurements were obtained across a two dimensional (2-D) 400 m × 60 m grid. Additional snow and ice thickness measurements collected in situ from adjacent ice floes helped to place the measurements obtained at the gridded survey field site into a more regional context. Widespread negative freeboards and flooding of the snow pack were observed during the N-ICE2015 expedition, due to the general situation of thick snow on relatively thin sea ice. These conditions caused brine wicking and saturation into the basal snow layers, causing more diffuse scattering and influenced the airborne radar signal to detect the radar main scattering horizon well above the snow/sea ice interface, resulting in a subsequent underestimation of total snow thickness, if only radar-based information is used. The average airborne snow thickness was 0.16 m thinner than that measured in situ at the 2-D survey field. Regional data within 10 km of the 2-D survey field suggested however a smaller deviation between average airborne and in situ snow thickness, a 0.06 m underestimate in snow thickness by the airborne radar, which is close to the resolution limit of the OIB snow radar system. Our results also show a broad snow thickness distribution, indicating a large spatial variability in snow across the region. Differences between the airborne snow radar and in situ measurements fell within the standard deviation of the in situ data (0.15 – 0.18 m). Our results suggest that, with frequent flooding of the snow-ice interface in specific regions of the Arctic in the future, it may result in an underestimate of snow thickness or an overestimate of ice freeboard, measured



from radar altimetry, thereby affecting the accuracy of sea ice thickness estimates.

35 **1 Introduction**

Snow and sea ice thickness in a changing Arctic climate system are the matter of many recent studies (e.g. Webster et al. 2018), since the snow layer on top of the frozen ocean generates several contradictory effects on the polar climate. On the one hand, in winter, snow acts as an insulator between the relatively warm ocean and the cold atmosphere and hinders the heat exchange between ocean and atmosphere, reducing the sea ice growth rate (Sturm, 2002; Perovich, 2003). On the other
40 hand, in spring and summer, with its high optical albedo in the range of 0.7-0.85, compared to about 0.6 for bare sea ice (Grenfell and Maykut, 1977, Perovich, 1996), Snow reflects short-wave radiation and prevents the underlying ice from melting. In addition, snow can be a positive contributor to the sea ice mass balance since snow can transform to snow-ice (Granskog et al., 2017; Merkouriadi et al., 2017a) and superimposed ice (Eicken et al., 2004; Wang et al., 2015).

Besides the importance of snow from a radiative and mass balance perspective, knowledge of snow thickness on sea ice is
45 also required for the accurate retrieval of sea ice thickness from satellite altimetry. The method relies on the assumption that sea ice floating in the ocean is in hydrostatic equilibrium, and sea ice thickness can be calculated by using observations of either ice-freeboard (from radar altimeters) or snow-freeboard (from laser altimeter) and assumptions about the respective densities of snow, ice and water. Ice- and snow-freeboard describe the distances above the local sea level to the snow/sea ice or air/snow interface, respectively. The error budget of the derived ice thickness from laser altimetry is
50 dominated by uncertainties of snow thickness and ice and snow densities, and as well as uncertainties due to remaining errors in the sea surface height (Giles et al., 2007; Kern et al., 2015; Skourup et al., 2017).

Thus, accurate knowledge of snow thickness on sea ice would be helpful to reduce the error in the sea ice thickness calculations and is important for quantifying climatological processes in Polar Regions. The Operation IceBridge (OIB) airborne campaigns (Koenig et al., 2010), which began in 2009, measure snow thickness and surface elevation with an
55 ultra-wideband snow radar (e.g., Yan et al., 2017) and an airborne topographic mapper (ATM) laser altimetry system (Krabill et al., 2002), respectively. With this constellation of sensors, both the air/snow and the snow/sea ice interface can be detected with the snow radar (e.g., Newman et al., 2014), and the surface elevation can be mapped with the ATM (e.g., Farrell et al., 2012). Hence, the OIB data are a valuable source for validating satellite remote sensing sea ice products as well as for model parameterization. Furthermore, the comparison of airborne OIB data with in situ field measurements is
60 necessary to understand the processes affecting radar penetration into snow covered sea ice and the impact of the snow load on the snow/sea ice interface.

Several OIB validation studies have been conducted (e.g., Farrell et al., 2012; Webster et al., 2014; Newman et al., 2014; Holt et al., 2015), multiple snow thickness retrieval algorithms were developed (e.g., Kurtz et al., 2013, 2014; Newman et al., 2014; Kwok and Maksym, 2014), and inter-compared with satellite products (Kwok et al., 2017; Lawrence et al., 2018).



65 These studies have provided insights about the snow thickness uncertainty and the errors associated with the airborne
techniques (Kwok, 2014; King et al., 2015). However, in the northern hemisphere, all evaluation studies (except those
connecting to satellite data) have thus far focused on snow in the Canada Basin, in the central Arctic Ocean, or only in
70 peripheral sub regions of the Arctic. To our knowledge, no OIB validation study has been conducted in the Atlantic sector
of the Arctic. In recent years, a significant change towards thinner ice with thicker snow cover (Renner et al., 2014; Rösel
et al., 2018) has been observed in this region, caused by an increase in intense storm events and associated precipitation in
this area (Woods and Caballero, 2016; Graham et al., 2017; Rinke et al., 2017). In addition, previous studies indicate that
radar signal penetration through the snow pack might be lower under certain geophysical snow-ice conditions in this area
(Gerland et al., 2013; King et al., 2018; Nandan et al., 2020) and also in the Weddell Sea ice in the Antarctic (Kwok and
75 Kacimi, 2018). Snow and ice conditions in this region differ to those in the Canada Basin and central Arctic (e.g., Webster
et al., 2014; 2018), and they have been found to induce substantial negative freeboards with subsequent flooding of the snow
pack, more akin to the conditions in the seasonal ice pack of the Southern Ocean (Massom et al., 2001). This may have an
impact on remote sensing methods of snow and ice thickness estimation, which have so far only been validated for more
typical Arctic conditions.

In this paper, we present in situ observations of sea ice and snow thickness, and snow and ice characteristics from the N-
80 ICE2015 expedition, alongside near-coincident airborne measurements acquired on 19 March 2015 during an OIB
overflight. We calculate ice freeboard values from a variety of sensors to investigate the prevalence of negative freeboards
and flooding at the snow/sea ice interface. We investigate the impact of flooded snow layers on the airborne radar observations.
Utilizing a combination of methodologies, we assess sea ice thickness conditions in the region. We discuss our results in the
context of satellite-derived ice thickness and consider the impact of flooding on estimating thickness in regions with thin
85 sea ice and deep snow, such as in the Southern Ocean or in the Atlantic sector of the Arctic Ocean.

2 Data and Methods

2.1 Study Area

Field observations for this study were acquired during the Norwegian young sea ICE expedition (N-ICE2015) with the
research vessel *RV Lance*. The expedition started in the Arctic Ocean north of Svalbard at 83°15'N, 21°32'E on 15 January
90 2015 and concluded at 80°N and 5°36'E on 22 June 2015 and consisted of a series of four drift segments (Granskog et al.,
2016, 2018). In this study, we focus on sea ice and snow related observations from the drift of *Floe 2*, covering a time period
from 24 February to 19 March 2015. Data from the OIB overflight employed in this study was collected on 19 March 2015
at 82°29'N and 22°37'E above the drifting sea ice floe.



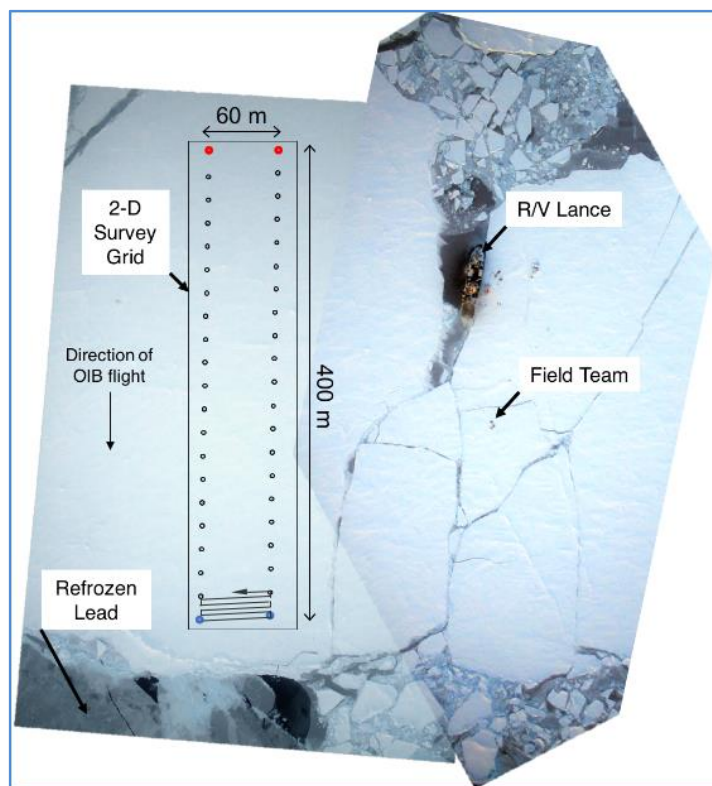
2.2 Ground-based measurements

95 The ice station on Floe 2 was set up on an aggregation of different ice types: refrozen leads, first year ice (FYI), and second
year ice (SYI). Modal sea ice thickness at the field station was 0.3 m, 0.9 m, and 1.7 m, for refrozen leads, FYI, and SYI,
respectively (Rösel et al., 2017). Snow thickness was on average 0.56 ± 0.17 m on FYI and SYI (Rösel et al., 2017), while
on refrozen leads it was approximately 0.02 m, likely redistributed from blowing snow. For this study, a $400 \text{ m} \times 60 \text{ m}$
100 survey field was established. Red flag poles, with black snow-filled trash bags, marked the outline making it visible from air
(see Figure 1). On this two dimensional (2-D) survey field, short after the overflights, snow thickness measurements (h_s ,
 $N=1121$) were obtained with a GPS snow probe (SP) from Snow-Hydro (Fairbanks, AK, USA). Total snow and ice
thickness measurements (h_t , $N=1046$) were obtained using the EM31 electromagnetic device (Geonics Ltd., Mississauga,
Ontario, Canada) within the 2-D survey field following a “snake line” sampling pattern with 5 m spacing (see Figure 1). The
snow probe is a thin pole with a sliding disk, 0.2 m in diameter. The pole penetrates the snow pack to the snow/sea ice
105 interface, while the disk rests on the snow surface. Inside the pole a magnetic device measures the distance between the disk
and the lower tip of the pole providing the snow thickness (Sturm and Holmgren, 1999; 2018). Each measurement is time-
tagged and geolocated, and recorded on a data logger. The accuracy of the measurements over sea ice may vary between ± 1 - 3
mm (Marshall et al., 2006; Sturm and Holmgren, 2018) and the footprint is the size of the disk (i.e., 0.2 m). Snow thickness
measurements were made approximately every 5 m following the snake line sampling pattern within the 2-D survey field (see
110 Figure 1). A person dragging the EM31 instrument on a plastic sledge followed the snow probe sampler. The EM31
measurements were sampled with a frequency of 2 Hz. The footprint size of the EM31 ranges from 3 m to 5 m (e.g., Haas et
al., 1997), depending on the ice and snow thickness. The accuracy of the EM31 measurements is approximately ± 0.1 m (Haas
et al., 2009) for level ice, but higher for rough and deformed ice. For comparison to the EM31 data and to collect direct
measurements, we drilled 10 equispaced holes with a 2" auger and measured ice and snow thickness, and ice freeboard with a
115 thickness gauge from Kovacs Enterprises (Roseburg, OR, USA). The gauge is a specific tape measure with a foldable metal
weight at the bottom that can be deployed through the drill-holes. The accuracy of the readings is estimated to be ± 0.01 m.
In addition, a snow pit was dug in the vicinity of the 2-D survey field (Merkouriadi et al., 2017c), and an ice core was
obtained to measure ice salinity, temperature, and density (Gerland et al., 2017). The core was extracted with a 0.09 m diameter
ice corer from Kovacs Enterprises (Roseburg, OR, USA). During the N-ICE2015 expedition a set of long, and independent,
120 transects with combined EM31 and snow thickness measurements ($N=5053$) were obtained within a maximum radius of 5 km
around the ship. These were performed to characterize the spatial variability of snow and ice thickness in the area
surrounding the main ice camp. Further details can be found in Rösel et al. (2018). We use the results of the independent snow
transects from *Floe 2* to provide the regional context for the measurements obtained in the smaller 2-D survey field.



2.3 Airborne measurements

125 The OIB aircraft surveyed the 2-D survey field three times (see Figure 2) on 19 March 2015. First a surveillance overflight
occurred at 15:28 UTC. A second and third pass directly over the 2-D survey field occurred at 15:37 UTC and 15:43 UTC,
respectively. Because the first pass did not adequately intersect the 2-D survey field, we focus our analysis on measurements
obtained during passes 2 and 3 of the aircraft. Although the ice floe drifted during the airborne survey, the alignment of transects
2 and 3 were such that they directly intersected the 2-D survey field on both passes. For sea ice studies, the aircraft was
130 equipped with an ATM laser altimeter system (Krabill et al., 2002), an ultra-wideband frequency modulated continuous
waveform (FMCW) snow radar system (e.g., Yan et al., 2017) and a digital camera system (DMS) that provides high-
resolution (0.1 m) geolocated visible-band images of the snow surface (Dominguez, 2018) allowing for visual interpretation
of sea ice conditions in the vicinity of the 2-D survey field (see Figure 1).



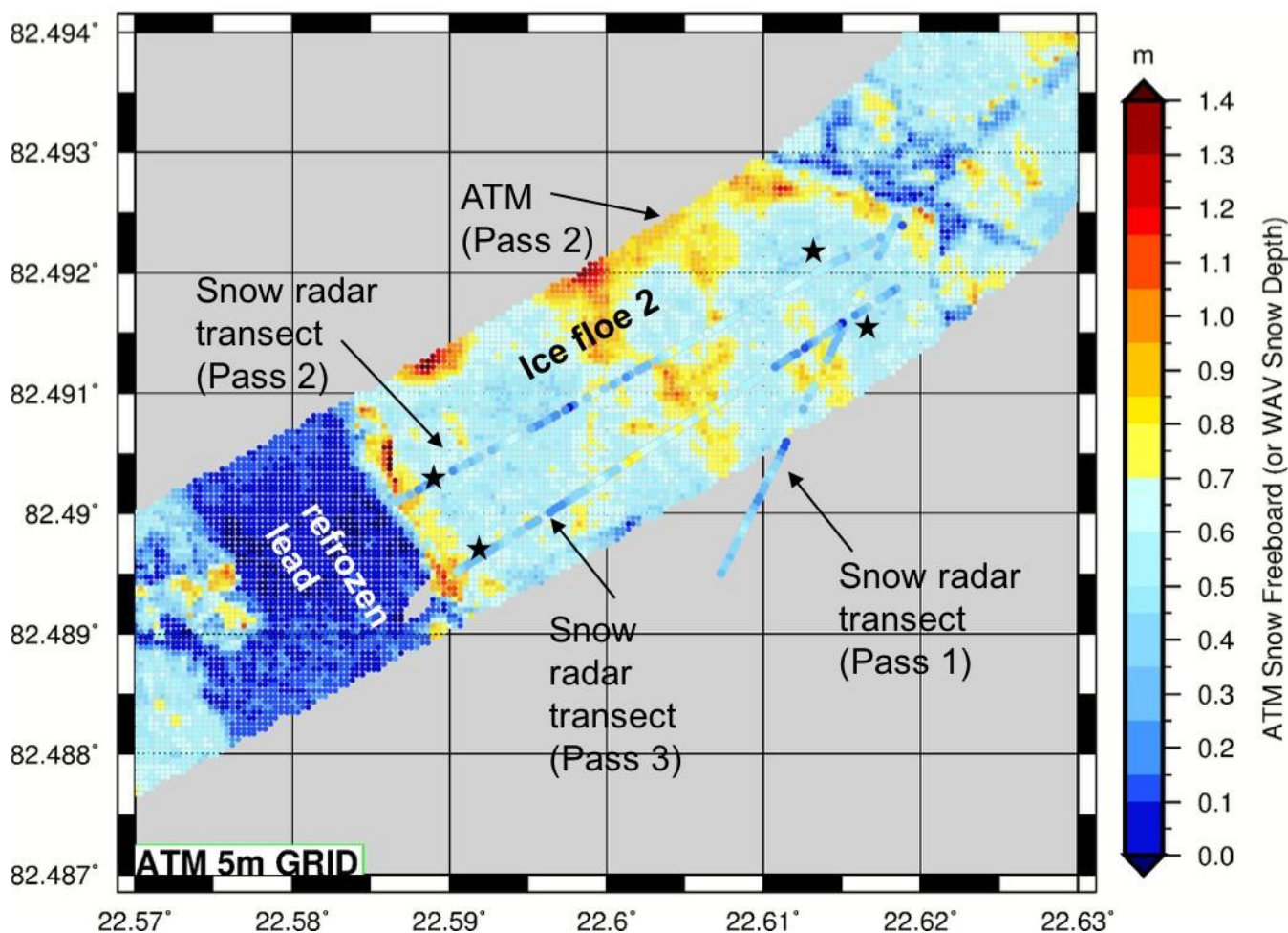
135

Figure 1. Overview of survey location and setup of the 2-D in situ survey field situated on an ice floe as a part of the *floe 2* drifting phase to the west of *R/V Lance* on March 19, 2015. Digital Mapping System (DMS) imagery (Dominguez, 2010, updated 2018) acquired during the OIB overflights were mosaicked to produce this overview map. Black dots indicate the



140 outline of the 2-D survey field. Snow and ice thickness measurements were obtained along the snake-line sampling pattern,
as indicated in the lower left of the figure.

145



150 **Figure 2.** Detailed airborne mapping of the snow freeboard (5 m grid, derived from ATM observations of surface elevation)
and snow thickness (superimposed dots, derived from the airborne snow radar) at the 2-D survey field (corner points



indicated by black stars) located on *Floe 2*. The three airborne transects across the field are indicated. During the survey, the ice floe drifted south at an approximate drift speed of 0.15 ms^{-1} .

155 2.4 Methodology

We number the variables measured with the different observation techniques as follows: 1) derived from in situ measurements with EM31 and SP; 2) derived from in situ measurements from drill holes; 3) derived from OIB measurements (ATM and snow radar); 4) derived from a combination of in situ and OIB measurements.

2.4.1 Drift correction

160 In order to obtain spatial coincidence between the in situ and airborne measurements of snow thickness, freeboard and sea ice thickness, and the positions of all measurements were first corrected to mitigate the impact of the drifting sea ice during the experiment. As a reference, we determined the position of the four corners of the 2-D survey field using the DMS imagery collected during the second and third OIB overpasses. We extracted the precise latitude and longitude from the geo-referenced DMS imagery and by comparing the differences for each corner marker between the two overpasses, we were able to deduce
165 that the ice floe was drifting south at a speed of 0.15 ms^{-1} . To correct for the drift that occurred during the EM31 and SP sampling of the 2-D survey field, we followed the procedure described in Rösel et al. (2018): The EM31 data was resampled onto the coordinates of the SP track, and a Gaussian filter was applied to the EM31 data. Afterwards, both the EM31 and the SP data were median-sampled on a 5 m regular grid to avoid oversampling (Geiger et al., 2015).

2.4.2 Density of sea water, ice and snow

170 In all calculations we used the following values: the density for sea water was $\rho_W = 1027 \text{ kgm}^{-3}$ (Meyer et al., 2017), the bulk density for the snow pack was $\rho_s = 328 \text{ kgm}^{-3}$ (Merkouriadi et al., 2017b), and the bulk density for FYI was $\rho_i = 910 \text{ kgm}^{-3}$ (Gerland et al., 2017). All values are based on actual measurements during the N-ICE2015 expedition at floe 2.

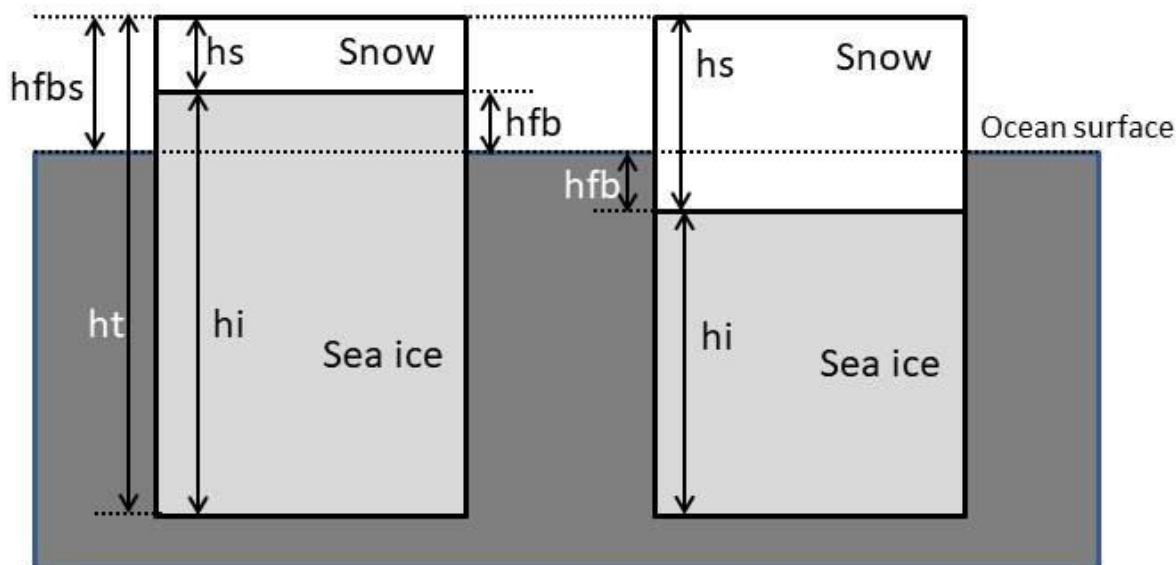
2.4.3 In situ snow thickness, sea ice thickness, and freeboards

In Figure 3, the concept of isostatic equilibrium is shown for two cases: On the left side, the ratio of snow thickness (h_s) to sea ice thickness (h_i) is small, resulting in a positive sea ice freeboard (hfb). On the right side, the situation of the 'new' Arctic as described in Rösel et al. (2018) is schematically presented: A thick snow layer h_s is pushing a relatively thin sea ice h_i layer below the ocean surface. The resulting sea ice freeboard hfb becomes negative, and subsequently the sea ice surface is vulnerable for flooding.



To obtain sea ice thickness (hi_{IS}) from the in situ measurements, the resampled snow thickness measurements from SP
 180 (hs_{SP} , $N=1046$) were subtracted from the total sea ice thickness from EM31 measurements (ht_{EM} , $N=1046$):

$$hi_{IS} = ht_{EM} - hs_{SP} \quad (1)$$



185

Figure 3: The concept of isostatic equilibrium of sea ice: On the left, the ratio of snow thickness (h_s) to sea ice thickness (h_i) is small, sea ice freeboard (hfb) is positive. On the right, the ratio of h_s to h_i is high, hfb is negative. Snow freeboard $hfbs$ is the same in both cases.

190 Assuming isostatic equilibrium assumption, hi_{IS} under dry snow conditions can be calculated as:

$$hi_{IS} = hfb_{IS} \left(\frac{\rho_W}{\rho_W - \rho_i} \right) - \left(\frac{\rho_W - \rho_s}{\rho_W - \rho_i} \right) hs_{SP} \quad (2)$$



195 which results in the freeboard ($hfb2_{IS}$) derived from the in situ (IS) measurements using obtained snow thickness and sea ice thickness information and densities given above:

$$hfb1_{IS} = \frac{hi1_{IS}(\rho_W - \rho_i) + (\rho_W - \rho_s)hs1_{SP}}{\rho_W} \quad (3)$$

200 For wet snow conditions, or a flooded state of the sea ice we refer to the studies of Zwally et al., 2008 and Ozsoy-Cicek et al., 2013 where either h_s is set equal to hfb_s , or a slush layer is included in the calculations, respectively. In addition, we gain in situ information from the drill-hole readings: Sea ice thickness ($hi2_{IS}$), snow thickness ($hs2_{IS}$), freeboard ($hfb2_{IS}$), and snow freeboard ($hsfb2_{IS}$)

$$hsfb2_{IS} = hfb2_{IS} + hs2_{IS} \quad (4)$$

205

The measurement accuracy of in situ freeboards $hfb1_{IS}$ and $hsfb1_{IS}$ is estimated to be ± 0.06 m; the accuracy of freeboard from the drill-hole measurements $hfb2_{IS}$ and $hsfb2_{IS}$ is ± 0.01 m (Rösel et al., 2018).

2.4.4 Airborne snow thickness, sea ice thickness, and freeboards

210 The DMS images were used to identify the geographical coordinates of areas of open water (with little or no ice cover) within the large refrozen lead, located in the southwest of the 2-D survey field site and adjacent to it (see Figure 1). ATM elevation measurements associated with these areas were averaged to estimate the local sea surface height (SSH). The SSH within the lead was then subtracted from all ATM elevations, to obtain the ATM snow freeboard ($hsfb3_{ATM}$). Individual ATM measurements were resampled on the same 5-m regular grid as the in situ snow and ice measurements across the sea ice floe (see Figure 2). The snow radar echoes from passes 2 and 3 from the OIB survey also illustrate the presence of open water, 215 refrozen leads and areas with deep snow cover on the N-ICE2015 ice floe (see Figure 4). We calculated snow thickness from snow radar ($hs3_{SR}$), following the methodology of Newman et al. (2014). Since the basal snow layers were saline in some locations, the snow/sea ice interface could not always be detected. Therefore, a running average at 25 m length-scale (equivalent to five snow radar measurements) was used to account for an observed diffuse snow-ice interface at the 2-D survey field site, possibly caused by a saline basal layer in the lower snow pack.

220

Ice freeboard ($hfb4_{ATM,SP}$) and sea ice thickness ($hi4_{ATM,SP}$) derived from a combination of the airborne data measurements acquired over the 2-D survey field site with the in situ snow-probe data were calculated as follows:

$$hfb4_{ATM,SP} = hsfb3_{ATM} - hs1_{SP} \quad (5)$$



225

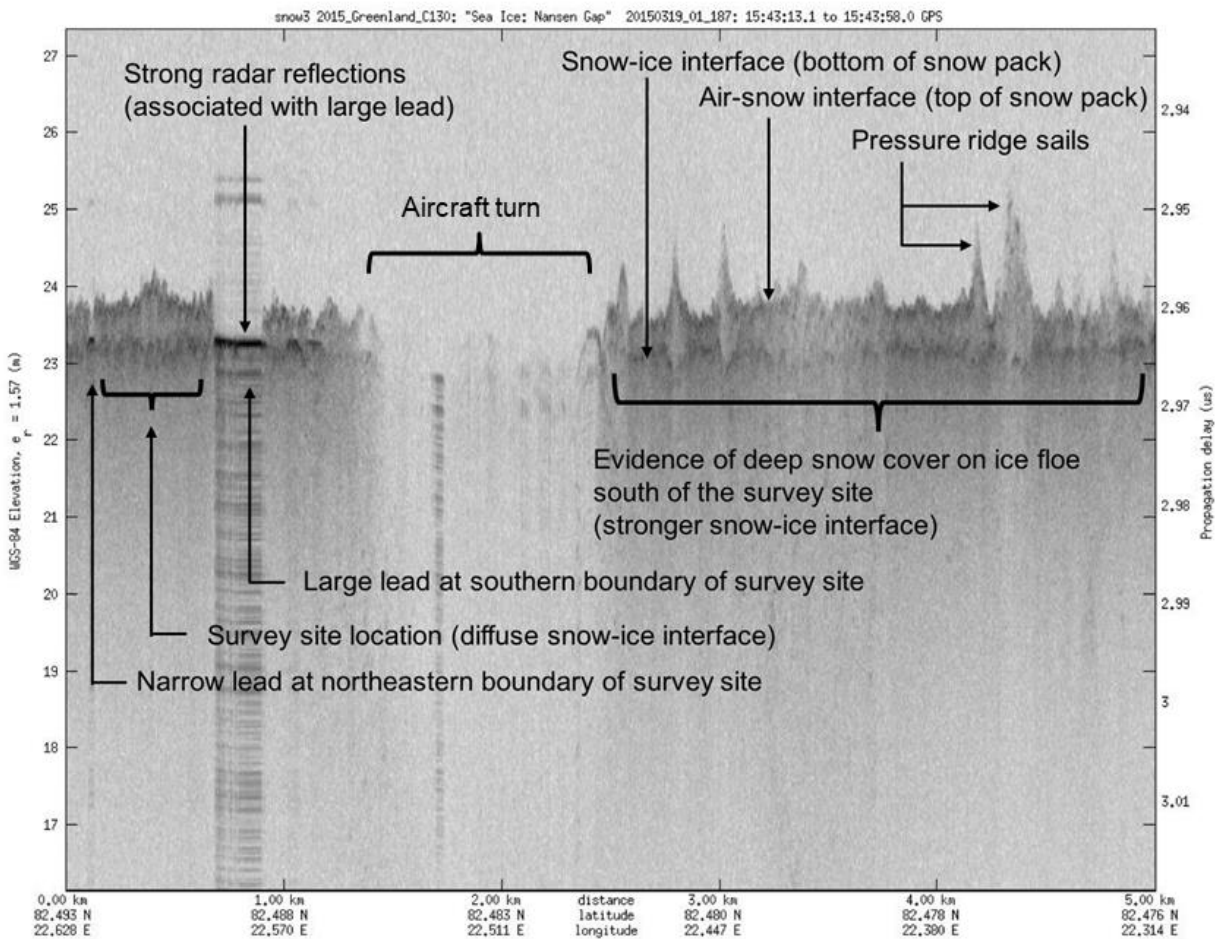
$$hi4_{ATM,SP} = \frac{\rho_W hfb4_{ATM,SP}}{\rho_W - \rho_i} + \frac{\rho_s hs1_{SP}}{\rho_W - \rho_i} \quad (6)$$

Here we introduce the term $hb3$ which is the difference between the ATM snow freeboard ($hsfb3_{ATM}$) and the snow radar snow thickness ($hs3_{SR}$). $hb3$ is used to indicate the depth of the ice freeboard plus the snow-ice basal layer, if present.

230

$$hb3_{ATM,SR} = hfb + hbsil + E = hsfb3_{ATM} - hs3_{SR} \quad (7)$$

Where hfb is the ice freeboard, $hbsil$ is the thickness of the snow-ice basal layer, and E is any remaining errors due to the interface picking algorithms as applied to the snow radar echos (Figure 4).



235



Figure 4: Processed and annotated OIB snow radar echo surveyed from the 2-D survey field, during the second and third pass on 19 March 2015. The second and third passes were acquired at 15:37 UTC and 15:43 UTC.

240 3 Results

The salinity profile of the ice core, taken on 5 March 2015 in the vicinity of the 2-D survey field site, shows a typical C-shape profile with relatively high salinity values up to 11.3 psu at the top and 5.8 psu at the bottom, respectively, and lower values of between 1.3 psu and 4.3 psu in the middle sections of the ice core (see Figure 10 in Appendix) suggesting that the 2-D survey field site on the ice floe comprised of FYI.

245 The average calculated sea-ice thicknesses ($hi1_{IS}$, eq. 1) on the 2-D survey field site is 1.50 ± 0.28 m with a mode of 1.40 m, and the average snow thickness measured with the snow probe is $hs1_{SP} = 0.58 \pm 0.15$ m with a mode of 0.55 m (results summarized in Table 1).

For direct comparison of the in situ sampled snow and ice thickness data, a subset of the snow radar data of both overpasses over the 2-D survey field site, limited by the 4 corner coordinates of the 2-D survey field ($N=227$), results in an
250 average snow thickness of $hs3_{SR} = 0.42 \pm 0.16$ m, with a second mode of 0.40 m, 0.16 m and 0.15 m lower than the mean and modal snow thickness of 0.55 m measured in situ at the 2-D survey field site, respectively ($N=1046$, Figure 5a). However, the standard deviations, i.e. the width and shape of the snow thickness distributions, for both the in situ and airborne snow radar observations are in very good agreement with values of 0.15 m and 0.16 m, respectively. In addition, the average snow thickness from the airborne snow radar was 0.08 m than average snow depth at the drill hole locations $hs2_{IS} =$
255 0.50 ± 0.18 m ($N=10$, Figure 5a).

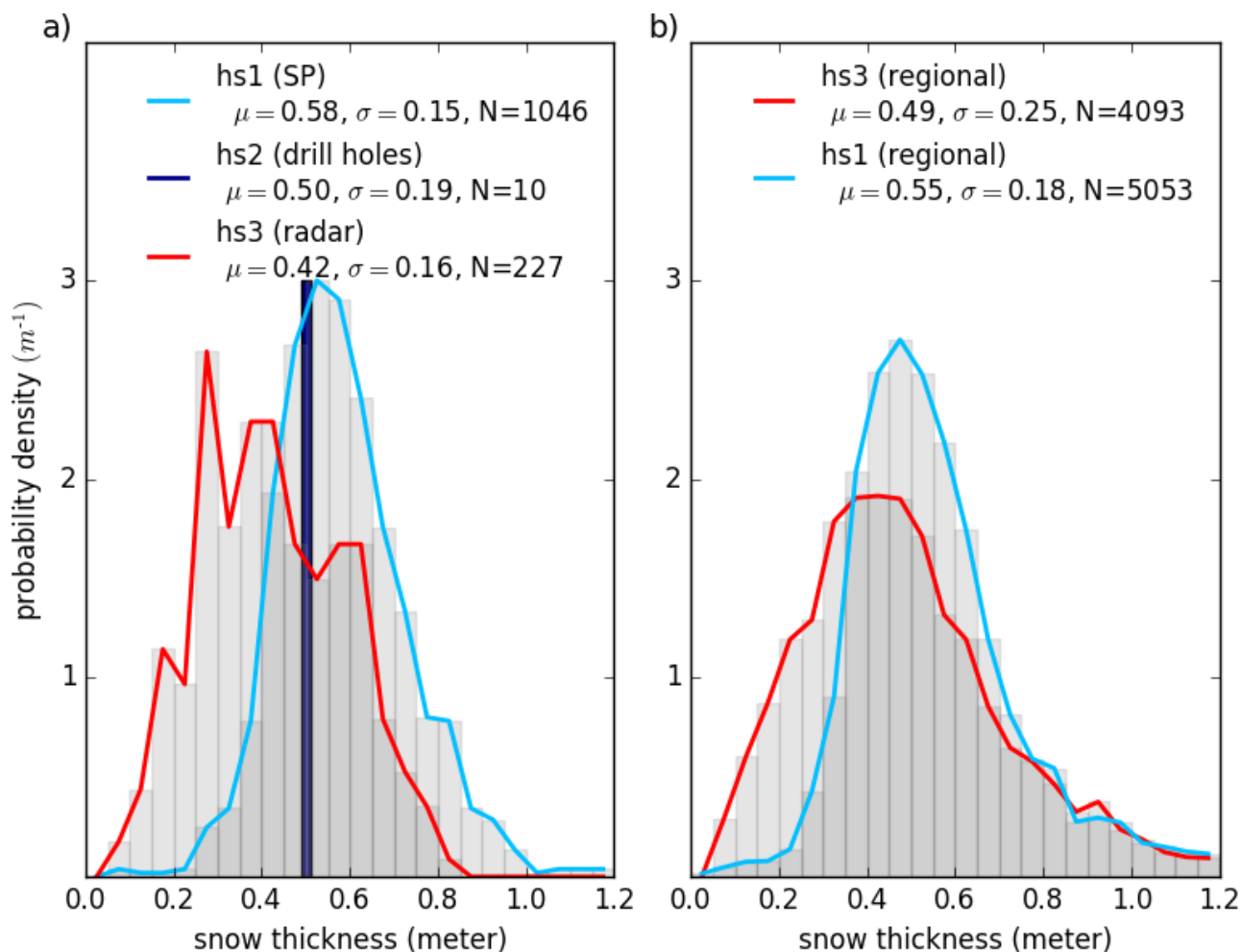
During the N-ICE2015 expedition, long transects on different predefined lines with combined EM31 and snow thickness measurements were performed to examine the spatial variability of the area surrounding the main ice camp and included measurements of thin ice and deformed ice areas (Rösel et al., 2018). Altogether, five transects with 5053 gridded snow and ice measurements were made on *Floe 2*, covering a time period from 24 February to 19 March 2015, which resulted in an
260 average snow thickness of 0.55 ± 0.18 m and an average sea ice thickness of 1.09 ± 0.92 m.

As shown in Rösel et al. (2017), the overall measurements on the local area scale are representative of sea ice in the region. To gain knowledge about the agreement in the snow thickness between the airborne and in situ observations on a more regional scale, we compared observations from snow radar within a 10 km radius around the position of *R/V Lance* with the average snow thickness conditions measured in situ during the drift of *Floe 2* during the N-ICE2015 expedition within a 5
265 km radius of the ship. Similar to the results obtained at the 2-D survey field site the snow distributions show an offset for the airborne snow radar data towards lower snow thickness values. The average snow thickness from the airborne snow radar was 0.49 ± 0.25 m, 0.06 m below the average snow thickness of 0.55 ± 0.18 m measured directly with the SP (Figure 5b).



270 While the one-to-one comparison over the survey field can be considered as a direct validation study, the statistical regional
comparison across the larger area can potentially be influenced by geophysical and thermodynamic processes such as ice
dynamics, snow redistribution, snow metamorphism etc. that occurred during the entire drift duration of *floe 2* (23 days)
where in situ data were acquired.

The drill-hole measurements made at the 2-D survey field site (N=10) gave the following averaged results: ice thickness
 $hi_{2_{IS}} = 1.39 \pm 0.33$ m, snow thickness $hs_{2_{IS}} = 0.50 \pm 0.18$ m, freeboard (FB2) $hfb_{2_{IS}} = 0.01 \pm 0.07$ m and snow freeboard
 $hsfb_{2_{IS}} = 0.50 \pm 0.12$ m (see Table 2 in Appendix). These values lie within the standard deviation of all measurements
275 collected at the 2-D survey field site, i.e. our results demonstrate very good agreement across all observation methods. Three
out of the ten drill-holes were flooded, already before drilling.



280

Figure 5. Probability density functions of snow thickness measurements with given average values (μ), standard deviations (σ), and number of measurements (N) from a) the in 2-D survey field site, obtained with the snow probe (blue) and the OIB snow radar (red) and b) a wider surrounding from snow probe in situ sampling during the entire N-ICE2015 - *floe 2* campaign (blue) and from OIB snow radar within a radius of 10 km around the position of *R/V Lance* (red).

285

For comparison with the ice freeboard, $hfb1_{IS} = 0.01 \pm 0.07$ m, observed at the drill hole sites, we used the in situ ground measurements, i.e. SP and EM31, to derive freeboard (FB1) $hfb1_{IS} = -0.02 \pm 0.05$ m with an uncertainty of ± 0.06 m (Rösel et al., 2018), following eqn. 3.

While the average freeboard at the 2-D survey field site is close to 0.00 m based on the drill hole measurements alone, the distribution of freeboards shown in Figure 5 illustrates that a significant fraction of $hfb1_{IS}$ values lie in the negative range, to -0.1 m. Results in the same range, with an average $hfb4_{ATM,SP} = 0.03 \pm 0.09$ m, are obtained by subtracting the snow

290



probe measurements from ATM surface elevation (FB4, see Figure 6). Taking the ± 0.06 m uncertainty into account, this results in a negative freeboard area fraction of 19% and 14% across the 2-D survey field site for FB1 and FB4, respectively (see Figure 7). An estimate of the ice freeboard plus the thickness of the snow-ice basal layer at the survey site that was impacted by brine wicking may be obtained by subtracting the snow radar measurements from the nearest ATM surface elevation value, which results in an average $hb3_{ATM,SR} = 0.20 \pm 0.10$ m but varies across the site (Figure 7c). The subsequent difference between $hb3_{ATM,SR}$ and $hfb4_{ATM,SP}$ provides an approximate estimate of the thickness of the flooded, snow-ice basal layer of the snow cover.

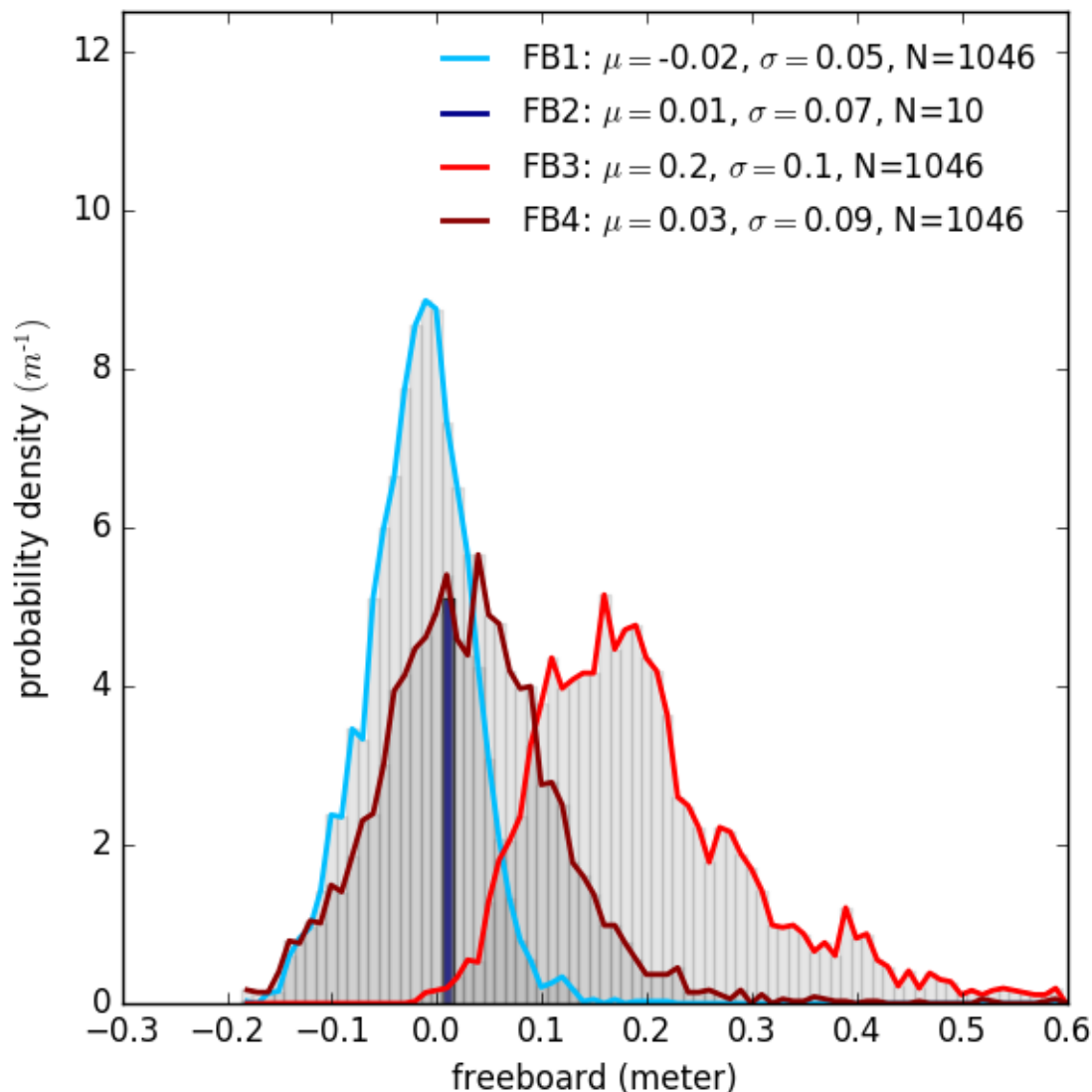
300

	snow thickness (h_s) [m]	sea ice thickness (h_i) [m]	snow freeboard $hsfb$ [m]	sea ice freeboard (hfb) [m]
(1) in situ (EM31/SP)	0.58 ± 0.15	1.50 ± 0.28	0.54 ± 0.09	-0.02 ± 0.05
(2) in situ (drill holes)	0.50 ± 0.18	1.39 ± 0.33	0.50 ± 0.12	0.01 ± 0.07
(3) OIB (Snow Radar)	0.42 ± 0.16			
(3) OIB (ATM)			0.62 ± 0.10	
(4) OIB (ATM/in situ)		1.90 ± 0.62		0.03 ± 0.09

Table 1: Results of snow, sea ice, and freeboard measurements and calculations of the 2-D survey field site

Finally, in Figure 8, we show the sea ice thickness distributions collected at the 2-D survey field site $hi1$ and $hi2$, as well as for the region surrounding the *R/V Lance*, $hi_{REGIONAL}$. For comparison we include $hi4$, calculated from a combination of the ATM data and the in situ snow probe measurements. The in situ measurements show that the 2-D survey field site was situated on an ice floe 1.4 to 1.5 m thick (Figure 8). This compares to a slightly thinner overall ice cover regionally (1.09 ± 0.92 m). The variability in sea ice thickness in the region surrounding the *R/V Lance* is about three times larger than that at the 2-D survey field site. We note that the average sea ice thickness $hi4 = 1.90$ m is biased high because the thickness equation (eqn. 6) does not take into account the two-layer snow set-up, with each snow layer having a different depth and density. Our results suggest that the resulting bias is approximately 0.4 m, and this is consistent with the result shown in Figure 6, which indicates a bias of approximately 0.03 m in FB1, which arose for the same reason (i.e., eqn. 2 also does not account for the two-layer snow situation).

310



315

Figure 6: PDFs of freeboards (FB) with given average values (μ), standard deviations (σ), and number of measurements (N) from the 2-D survey field site. FB1 (light blue): Freeboard calculated from SP snow thickness, sea ice thickness from EM31 and densities of snow, ice and water, and assuming a hydrostatic equilibrium sea ice thickness; FB2 (dark blue): Freeboard from drill hole measurements; FB3 (red): Freeboard derived from ATM surface elevation minus average snow thickness of SR measurements; FB4 (dark red): Freeboard derived from ATM surface elevation minus snow thickness of SP measurements. Detailed descriptions of the methods are given in the text.

320

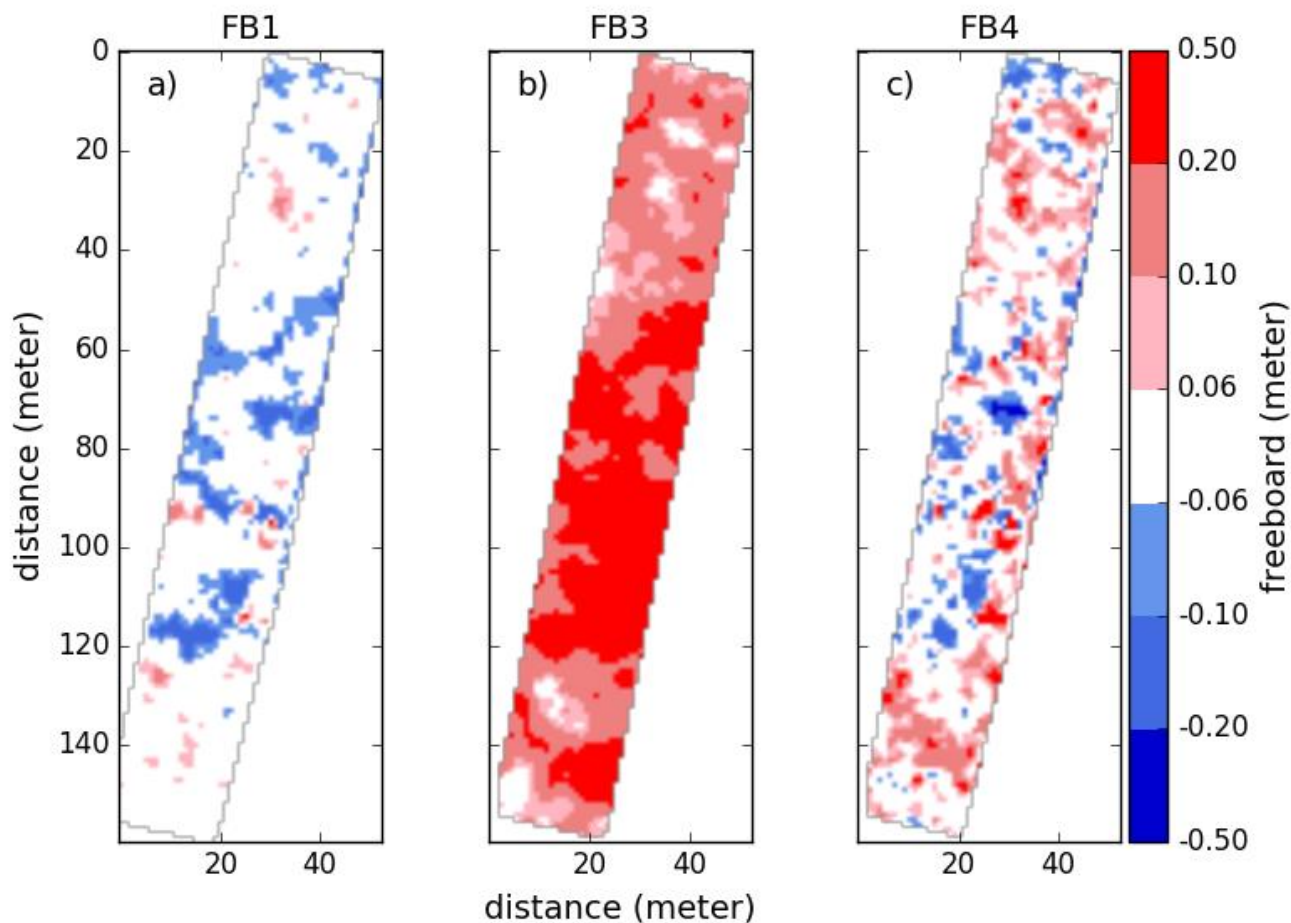


Figure 7. Freeboards (FB) over the 2-D survey field site. a) FB1 (calculated from SP snow thickness, sea ice thickness from EM31 and densities of snow, ice and water), b) FB3 (surface elevation from ATM minus snow thickness from SR), c) FB4 (surface elevation from ATM minus snow thickness from SR) of the 2-D survey field site. The white range represents the uncertainty of the freeboard estimation for FB1 ($\pm 0.06\text{m}$) and is also applied for FB3 and FB4.

330



335

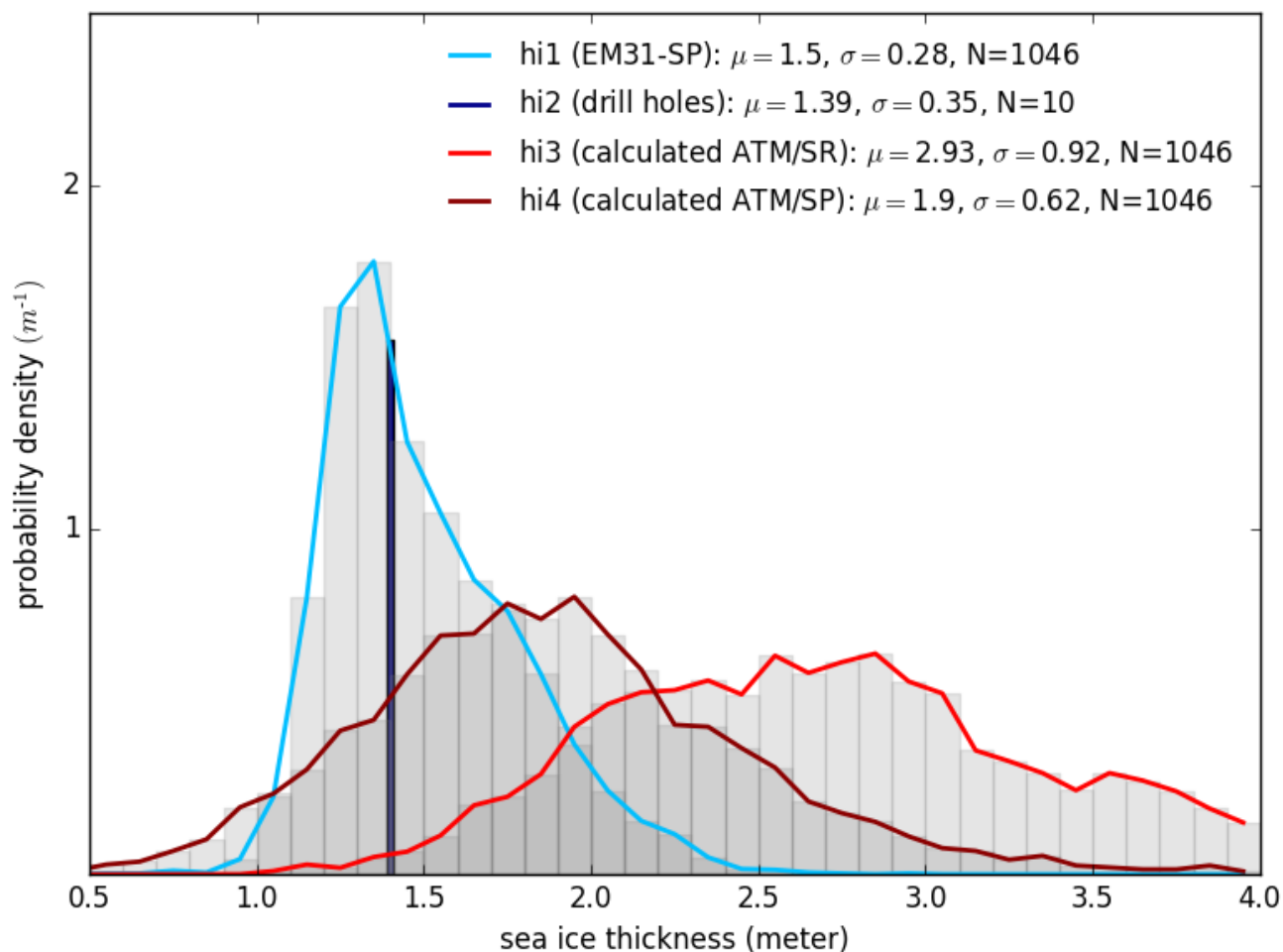


Figure 8: PDFs of sea ice thickness (h_i) with given average values (μ), standard deviations (σ), and number of measurements (N) from the 2-D survey field site. $hi1$ (light blue): Ice thickness calculated from EM31 total thickness and SP snow thickness; $hi2$ (dark blue): Ice thickness from drill hole measurements; $hi3$ (red): Ice thickness derived from ATM surface elevation and average snow thickness of SR measurements; $hi4$ (dark red): Ice thickness derived from ATM surface elevation and snow thickness of SP measurements. Detailed descriptions of the methods are given in the text.

340

4 Discussion and Conclusions

The mean and modal snow thickness estimates derived from the snow radar were 0.15-0.16 m lower than the in situ snow probe measurements, obtained at the 2-D survey field site. Over a larger regional scale of 10 km radius about the *R/V Lance*

345



location, snow thickness estimates derived from the snow radar underestimate in situ snow probe-derived thickness by 0.06 m, which is close to the measurement uncertainty of the snow radar system associated with its range resolution (Newman et al., 2014).

In radar altimetry, it is assumed that the radar signal penetrates completely through a dry snow pack and energy is reflected from the snow/sea ice interface, which represents the height of the sea ice-freeboard above local sea level. This assumption is valid (Beaven et al., 1995) for a cold, dry and homogenous snow pack, typical of Arctic sea ice in winter. However, for snow packs exhibiting high moisture content or higher densities (e.g. due to ice lenses/crusts), radar signals undergo absorption within the snow volume (e.g., Kwok and Maksym, 2014; Ricker et al., 2015). Recent studies suggest reduced signal penetration into the snow pack, with a more diffuse snow/sea ice interface, on both Arctic and Antarctic sea ice (Gerland et al., 2013; Kwok and Kacimi, 2018), especially if the snow pack is saline (Nandan et al., 2020; Nandan et al., 2017) or very deep with ice lenses present (King et al., 2018). In addition, deep snow pushes the ice surface below the water level, leading to negative freeboard and induces flooding and slushy, snow-ice formation in the basal layers of the snow pack, which, when measured with a radar altimeter system, can result in a dominant scattering horizon above the true snow/ice interface (Nandan et al., 2020), and hence an overestimation of ice freeboard and thus sea ice thickness, and an underestimate of total snow thickness.

On FYI, overlying snow also wicks brine upwards from the sea ice surface during freeze-up, producing saline snow layers, predominately observed in the bottom-most 0.06-0.08 m of the snow pack (Drinkwater and Crocker, 1988; Geldsetzer et al., 2009; Nandan et al., 2016, 2017, 2020). Sea ice salinity observations from the 1-m thick FYI floe, collected on 5 and 23 March 2015, show salinities of > 11 psu in the uppermost 0.10 m sea ice layers (Figure 10 in Appendix). Snow salinity observations from snow covers (0.26 m and 0.34 m thick) overlying the FYI floe indicate highly-saline, 0.10 m deep basal layers in both snow covers, by up to 10 psu. Additionally, one-third of the drill-holes at the 2D field site indicated flooding of the snow pack, and negative freeboard, which induced the formation of highly saline and saturated slush in the basal snow layers. The presence of this slushy snow-ice layer at the 2D field site resulted in a challenging geophysical setting for the measurement of total snow and ice thickness using remote sensing techniques.

Previous studies (Barber et al., 1998; Barber and Nghiem, 1999; Nghiem et al., 1995; Geldsetzer et al., 2009; Nandan et al., 2017; Nandan et al., 2020) have reported the impact of saline snow on FYI, which alters the geophysical, thermodynamic, dielectric and radar scattering properties of the snow cover, thereby impacting radar signal penetration through the snow pack. Nandan et al. (2017) and (2020) showed that a saline snow cover on a FYI setting, induced by upward brine wicking from the sea ice surface, shifted the main radar scattering horizon away from the snow/sea ice interface by up to 0.07 m, and weakened the signal arising from the saline scattering horizon. In these studies, covering the Canadian (Nandan et al., 2017) and the Atlantic (Nandan et al., 2020) sectors of the Arctic, the conditions at the survey field site included saline, wet, and deep snow which impacted the accuracy of the snow thickness derived from the snow radar signal. In the Nandan et al. (2020) case study from the N-ICE2015 experiment, they demonstrated significant overestimations in FYI thickness by up to 95%



380 between simulated FYI thickness, snow radar and ATM-derived FYI thickness. They simulated the Ku-band radar scattering horizon from 0.36 m and 0.45 m deep snow on 0.69 m and 0.92 m thin ice, exhibiting negative freeboards by 0.04 m and 0.07 m, respectively. They found that the FYI thickness overestimations was a result of vertical shift in the radar scattering horizon, caused by brine wicking from the slushy snow layers, caused by negative freeboards.

Our study shows that saline snow conditions can lead to the observed underestimation of total snow thickness by the radar, due to a combination of factors including reflection from a scattering horizon in the snow pack that is above the main
385 snow/ice interface, a diffuse scattering horizon within the snow volume, and potential errors in the height of the snow/ice interface picked in individual snow radar echoes. Even though the snow radar underestimated mean snow thickness by between 0.06 m and 0.16 m across the 2-D survey field site and the regional survey, the radar was able to fully reproduce the snow thickness variability, when compared to in situ measurements (standard deviations of 0.16 m and 0.15 m for the survey field, respectively; see Figure 3). Thus, we can report that the airborne snow radar is capable of measuring meaningful snow
390 thickness distributions even in challenging snow pack conditions. However, ambiguous radar signal penetration through slushy layers (caused by sea ice flooding) and saline snow covers (caused by brine wicking from sea ice surface) may introduce a potential bias in accurate estimates of total snow thickness. For a radar altimeter, the main scattering horizon within the snow volume is not just a function of snow thickness, but also depends on the thermodynamic properties of the snow cover (i.e., snow temperature, density, salinity, wetness, roughness, and grain microstructure). Further research is
395 required to understand the relationship between the main scattering horizon and variability in snow cover properties.

Biases caused by uneven penetration of radar altimeter signals within slushy and saline layers in the snow pack will also have implications on estimates of snow and sea ice thickness measurements from currently operational satellite-based radar altimeters such as SARAL AltiKa (Ka-band), CryoSat-2 and Sentinel-3A/B (Ku-band), and the ESA's upcoming Ku- and Ka-band dual-frequency satellite radar altimeter mission CRISTAL. King et al. (2018) reported underestimation of sea ice
400 thickness derived from CryoSat-2 data caused by negative freeboards in the same region as was investigated in our study. A detailed quantification of the contributions to the error budget associated with freeboard retrieval from CryoSat-2 was made by the ESA CryoVal-SI project team and is described in Ricker et al. (2014) and Haas et al. (2016). To examine the impact of a deep snow pack with saline and/or flooded snow-ice interface, we show as an example the CryoSat-2 sea ice products provided by the NASA Goddard Space Flight Center (GSFC, Kurtz et al., 2014) for the region surrounding *R/V Lance*
405 location in March 2015 (Figure 9). It is striking that for this region the CryoSat-2 sea ice freeboard is up to 0.3 m (Figure 9b), and the derived sea ice thickness is overestimated by over 1.0 m (Figure 9c), when compared with the in situ results reported in Rösel et al., 2018). The assumed snow thicknesses of 0.15 m and 0.37 m (derived from Warren et al., 1999; Kurtz et al., 2014, Figure 9a) are underestimated when compared to the observed in situ snow thickness, which averaged 0.55 m. Sea ice parameters from the GSFC CryoSat-2 are derived with a waveform fitting procedure using an empirical waveform
410 model (Sallila et al., 2019), which should account for snow geophysical properties. But, to our knowledge, currently, none of the conventional CryoSat-2 retracker algorithms (Hendricks et al. 2010; Ricker et al., 2014) or the empirical models (Kurtz



et al., 2014) include flooding in the snow pack as a consideration. This issue could cause misinterpretation of both, airborne and satellite radar altimeter signals especially in areas where flooding of the snow cover has been observed such as in the Atlantic sector of the Arctic, and also in parts of the Weddell and Bellingshausen Seas in the Southern Ocean which results in an overestimation of sea ice thickness. Our study suggests that this issue should be considered and improved in the future.

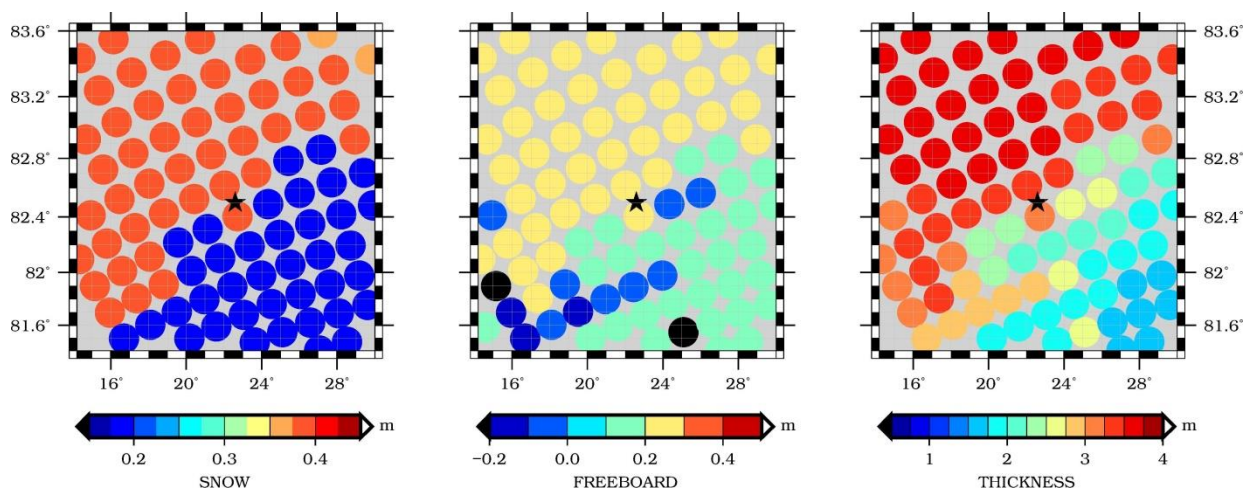


Figure 9: Results from CryoSat-2 sea ice products from GSFC, averaged for the month March 2015 for a region of 250 km × 250 km over the in-situ site in the Norwegian Arctic for a) snow thickness, b) sea ice freeboard, c) sea ice thickness. The position of *R/V Lance* is marked with a star.

Acknowledgements: We thank all crew members of *R/V Lance* and all scientific staff involved in N-ICE2015 for their support and help during the fieldwork. This work was supported by the Norwegian Polar Institute’s Center for Ice, Climate and Ecosystems (ICE) through the project N-ICE2015 and the project ID Arctic (Norwegian Ministries of Foreign Affairs and Environment; SG, AR). VN acknowledges Post-Doctoral Fellowship grant to Canada’s Marine Environmental Observation, Prediction and Response Network (MEOPAR). SLF was supported under NOAA grant NA14NES4320003, and the NOAA Product Development, Readiness, and Application (PDRA)/Ocean Remote Sensing (ORS) program. GS acknowledges support by the Trans regional Collaborative Research Center (TR 172) “Arctic Amplification: Climate Relevant Atmospheric and SurfaCe Processes, and Feedback Mechanisms (AC)3”, funded by the German Research Foundation DFG. N-ICE2015 acknowledges the in-kind contributions provided by other national and international projects and participating institutions, through personnel, equipment and other support. N-ICE2015 data is



available through <http://data.npolar.no/> and NASA's OIB data is publicly available via
435 <https://nsidc.org/icebridge/portal/map>.

References

- Barber, D., Fung, A., Grenfell, T., Nghiem, S., Onstott, R., Lytle, V., Perovich, D., and Gow, A.: The Role of Snow on Microwave Emission and Scattering over First-Year Sea Ice, *IEEE Transactions on Geoscience and Remote Sensing*, 36, 1750–1763, 1998.
- 440 Barber, D. G. and Nghiem, S. V.: The role of snow on the thermal dependence of microwave backscatter over sea ice, *Journal of Geophysical Research: Oceans*, 104, 25 789–25 803, 1999.
- Beaven, S. G., Lockhart, G. L., Gogineni, S. P., Hossetnmostafa, A. R., Jezek, K., Gow, A. J., Perovich, D. K., Fung, A. K., and Tjuatja, S.: Laboratory measurements of radar backscatter from bare and snow-covered saline ice sheets, *International Journal of Remote Sensing*, 16, 851–876, 1995.
- 445 Dominguez, R.: Icebridge DMS L1B geolocated and orthorectified images, (IODMS1B), Boulder, Colorado USA. NASA National Snow and Ice Data Center Distributed Active Archive Center., 2010, updated 2018.
- Drinkwater, M. R. and Crocker, G.: Modelling Changes in Scattering Properties of the Dielectric and Young Snow-Covered Sea Ice at GHz Frequencies, *Journal of Glaciology*, 34, 274–282, 1988.
- Eicken, H., Grenfell, T. C., Perovich, D. K., Richter-Menge, J. A., and Frey, K.: Hydraulic controls of summer Arctic pack ice
450 albedo, *Journal of Geophysical Research: Oceans*, 109, 2004.
- Farrell, S. L., Kurtz, N., Connor, L. N., Elder, B. C., Leuschen, C., Markus, T., McAdoo, D. C., Panzer, B., Richter-Menge, J., and Sonntag, J. G.: A First Assessment of IceBridge Snow and Ice Thickness Data Over Arctic Sea Ice, *IEEE Transactions on Geoscience and Remote Sensing*, 50, 2098–2111, 2012.
- Geiger, C., Müller, H.-R., Samluk, J. P., Bernstein, E. R., and Richter-Menge, J.: Impact of spatial aliasing on sea-ice thickness
455 measurements, *Annals of Glaciology*, 56, 53–362, 2015.
- Geldsetzer, T., Langlois, A., and Yackel, J.: Dielectric properties of brine-wetted snow on first-year sea ice, *Cold Regions Science and Technology*, 58, 47–56, 2009.
- Gerland, S., Renner, A. H. H., Spreen, G., Wang, C., Beckers, J., Dumont, M., Granskog, M. A., Haapala, J., Haas, C., Helm, V., Hudson, S. R., Lensu, M., Ricker, R., Sandven, S., Skourup, H., and Zygmuntowska, M.: In-situ calibration and
460 validation of CryoSat-2 Observations Over Arctic sea ice north of Svalbard, in: *Proc. Earth Observation and Cryosphere Science Conf.*, Frascati, Italy, 13-16 November 2012, ESA SP-712, 2013.
- Gerland, S., Granskog, M. A., King, J., and Rösel, A.: [data set] N-ICE2015 ice core physics: temperature, salinity and density, <https://doi.org/10.21334/npolar.2017.c3db82e3>, 2017.



- Giles, K.A., Laxon, S.W., Wingham, D.J., Wallis, D.W., Krabill, W.B., Leuschen, C.J., McAdoo, D., Manizade, S.S. and
465 Raney, R.K., 2007. Combined airborne laser and radar altimeter measurements over the Fram Strait in May 2002. *Remote
Sensing of Environment*, 111(2-3), pp.182-194.
- Graham, R. M., Cohen, L., Petty, A. A., Boisvert, L. N., Rinke, A., Hudson, S. R., Nicolaus, M., and Granskog, M. A.:
Increasing frequency and duration of Arctic winter warming events, *Geophysical Research Letters*, 44, 6974–6983, 2017.
- Granskog, M., Assmy, P., Gerland, S., Spreen, G., Steen, H., and Smedsrud, L.: Arctic Research on Thin Ice: Consequences
470 of Arctic Sea Ice Loss, *Eos, Transactions American Geophysical Union*, 97, 2016.
- Granskog, M. A., Rösel, A., Dodd, P. A., Divine, D., Gerland, S., Martma, T., and Leng, M. J.: Snow contribution to first-
year and second-year Arctic sea ice mass balance north of Svalbard, *Journal of Geophysical Research: Oceans*, 122, 2539–
2549, 2017.
- Grenfell, T. C. and Maykut, G. A.: The Optical Properties of Ice and Snow in the Arctic Basin, *Journal of Glaciology*, 18,
475 445–463, 1977.
- Haas, C., Gerland, S., Eicken, H., and Miller, H.: Comparison of sea-ice thickness measurements under summer and winter
conditions in the Arctic using a small electromagnetic induction device, *GEOPHYSICS*, 62, 749–757, 1997.
- Haas, C., Lobach, J., Hendricks, S., Rabenstein, L., and Pfaffling, A.: Helicopter-borne measurements of sea ice thickness,
using a small and lightweight, digital EM system, *Journal of Applied Geophysics*, 67, 234–241, 2009.
- 480 Haas, C., Hendricks, S., Ricker, R., King, J., Beckers, J. and Skourup, H., and et al.: CryoVal-SI: CryoSat Sea Ice Product
Validation using CryoVex and IceBridge campaign data, Techreport, Norwegian Polar Institute, 2016.
- Hendricks, S., Stenseng, L., Helm, V., and Haas, C.: Effects of Surface Roughness on Sea Ice Freeboard Retrieval with an
Airborne Ku-Band SAR Radar Altimeter, in: *Geoscience and Remote Sensing (IGARSS 2010)*, IEEE International
Symposium., 2010.
- 485 Holt, B., Johnson, M. P., Perkovic-Martin, D., and Panzer, B.: Snow depth on Arctic sea ice derived from radar: In situ
comparisons and time series analysis, *Journal of Geophysical Research: Oceans*, 120, 4260–4287, 2015.
- Kern, S., Khvorostovsky, K., Skourup, H., Rinne, E., Parsakhoo, Z. S., Djepa, V., Wadhams, P., and Sandven, S.: The
impact of snow depth, snow density and ice density on sea ice thickness retrieval from satellite radar altimetry: results from
the ESA-CCI Sea Ice ECV Project Round Robin Exercise, *The Cryosphere*, 9, 37–52, 2015.
- 490 King, J., Howell, S., Derksen, C., Rutter, N., Toose, P., Beckers, J. F., Haas, C., Kurtz, N., and Richter-Menge, J.:
Evaluation of Operation IceBridge quick-look snow depth estimates on sea ice, *Geophysical Research Letters*, 42, 9302–
9310, 2015.
- King, J., Skourup, H., Hvidegaard, S. M., Rösel, A., Gerland, S., Spreen, G., Polashenski, C., Helm, V., and Liston, G. E.:
495 Comparison of Free- board Retrieval and Ice Thickness Calculation From ALS, ASIRAS, and CryoSat-2 in the Norwegian



- Arctic to Field Measurements Made During the N-ICE2015 Expedition, *Journal of Geophysical Research: Oceans*, 123, 1123–1141, 2018.
- Koenig, L., Martin, S., Studinger, M., and Sonntag, J.: Polar Airborne Observations Fill Gap in Satellite Data, *Eos, Transactions American Geophysical Union*, 91, 333–334, 2010.
- 500 Krabill, W., Abdalati, W., Frederick, E., Manizade, S., Martin, C., Sonntag, J., Swift, R., Thomas, R., and Yungel, J.: Aircraft laser altimetry measurement of elevation changes of the greenland ice sheet: technique and accuracy assessment, *Journal of Geodynamics*, 34, 357–376, 2002.
- Kurtz, N. T., Farrell, S. L., Studinger, M., Galin, N., Harbeck, J. P., Lindsay, R., Onana, V. D., Panzer, B., and Sonntag, J. G.: Sea ice thickness, freeboard, and snow depth products from Operation IceBridge airborne data, *The Cryosphere*, 7, 1035–
505 1056, 2013.
- Kurtz, N. T., Galin, N., and Studinger, M.: An improved CryoSat-2 sea ice freeboard retrieval algorithm through the use of waveform fitting, *The Cryosphere*, 8, 1217–1237, <https://doi.org/10.5194/tc-8-1217-2014>, 2014.
- Kwok, R.: Simulated effects of a snow layer on retrieval of CryoSat-2 sea ice freeboard, *Geophysical Research Letters*, 41, 5014–5020, 2014.
- 510 Kwok, R. and Kacimi, S.: Three years of sea ice freeboard, snow depth, and ice thickness of the Weddell Sea from Operation IceBridge and CryoSat-2, *The Cryosphere*, 12, 2789–2801, 2018.
- Kwok, R. and Maksym, T.: Snow depth of the Weddell and Bellingshausen sea ice covers from IceBridge surveys in 2010 and 2011: An examination, *Journal of Geophysical Research: Oceans*, 119, 4141–4167, 2014.
- Kwok, R., Kurtz, N. T., Brucker, L., Ivanoff, A., Newman, T., Farrell, S. L., King, J., Howell, S., Webster, M. A., Paden, J.,
515 Leuschen, C., Macgregor, J. A., Richter-Menge, J., Harbeck, J., and Tschudi, M.: Inter-comparison of snow depth retrievals over Arctic sea ice from radar data acquired by Operation IceBridge, *The Cryosphere*, 11, 2571–2593, 2017.
- Lawrence, I.R., Tsamados, M.C., Stroeve, J.C., Armitage, T.W.K., and Ridout, A.L.: Estimating snow depth over Arctic sea ice from calibrated dual-frequency radar freeboards. *The Cryosphere*, 12, 3551–3564, 2018.
- Marshall, H. P., Koh, G., Sturm, M., Johnson, J., Demuth, M., Landry, C., Deems, J., and Gleason, A.: Spatial variability of
520 the snowpack: Experiences with measurements at a wide range of length scales with several different high precision instruments, *Proc. ISSW 2006*, pp. 359–364, 2006.
- Massom, R. A., Eicken, H., Hass, C., Jeffries, M. O., Drinkwater, M. R., Sturm, M., Worby, A. P., Wu, X., Lytle, V. I., Ushio, S., Morris, K., Reid, P. A., Warren, S. G., and Allison, I.: Snow on Antarctic sea ice, *Reviews of Geophysics*, 39, 413–445, 2001.
- 525 Merkouriadi, I., Cheng, B., Graham, R. M., Rösel, A., and Granskog, M. A.: Critical Role of Snow on Sea Ice Growth in the Atlantic Sector of the Arctic Ocean, *Geophysical Research Letters*, 44, 10,479–10,485, 2017a.
- Merkouriadi, I., Gallet, J.-C., Liston, G., Polashenski, C., Itkin, P., King, J., Espeseth, M., Gierisch, A., Oikkonen, A., Orsi, A., and Gerland, S.: [data set] N-ICE2015 snow pit data, <https://doi.org/10.21334/npolar.2017.d2be5f05>, 2017b.



- Merkouriadi, I., Gallet, J.-C., Liston, G. E., Polashenski, C., Rösel, A., and Gerland, S.: Winter snow conditions over the Arctic Ocean north of Svalbard during the Norwegian young sea ICE (N-ICE2015) expedition, *Journal of Geophysical Research: Atmospheres*, 122, 2017c.
- Meyer, A., Sundfjord, A., Fer, I., Provost, C., Robineau, N. V., Koenig, Z., Onarheim, I. H., Smedsrud, L. H., Duarte, P., Dodd, P. A., Graham, R. M., and Kauko, H.: Winter to summer hydrographic and current observations in the Arctic Ocean north of Svalbard, *Journal of Geophysical Research: Oceans*, 122, 2017.
- 535 Nandan, V., Scharien, R. K., Geldsetzer, T., Kwok, R., Yackel, J. J., Mahmud, M., Rösel, A., Tonboe, R., Granskog, M., Willatt, R., Stroeve, J., Nomura, D and Frey, M. "Snow Property Controls on Modeled Ku-Band Altimeter Estimates of First-Year Sea Ice Thickness: Case Studies from the Canadian and Norwegian Arctic," in *IEEE Journal of Selected Topics in Applied Earth Observations and Remote Sensing*, 13, 1082-1096, 2020.
- Nandan, V., Geldsetzer, T., Islam, T., Yackel, J. J., Gill, J. P., Fuller, M. C., Gunn, G., and Duguay, C.: Ku-, X- and C-band
540 measured and modeled microwave backscatter from a highly saline snow cover on first-year sea ice, *Remote Sensing of Environment*, 187, 62 – 75, 2016.
- Nandan, V., Geldsetzer, T., Yackel, J., Mahmud, M., Scharien, R., Howell, S., King, J., Ricker, R., and Else, B.: Effect of Snow Salinity on CryoSat-2 Arctic First-Year Sea Ice Freeboard Measurements, *Geophysical Research Letters*, 2017.
- Newman, T., Farrell, S. L., Richter-Menge, J., Connor, L. N., Kurtz, N. T., Elder, B. C., and McAdoo, D.: Assessment of
545 radar-derived snow depth over Arctic sea ice, *Journal of Geophysical Research: Oceans*, 119, 8578–8602, 2014.
- Nghiem, S. V., Kwok, R., Yueh, S. H., and Drinkwater, M. R.: Polarimetric signatures of sea ice: 2. Experimental observations, *Journal of Geophysical Research: Oceans*, 100, 13 681–13 698, 1995.
- Ozsoy-Cicek, B., Ackley, S., Xie, H., Yi, D., and Zwally, J.: Sea ice thickness retrieval algorithms based on in situ surface elevation and thickness values for application to altimetry, *Journal of Geophysical Research: Oceans*, 118, 3807– 3822,
550 2013.
- Perovich, D. K.: *The Optical Properties of Sea Ice*, vol. 96, CRREL Monography, 1996. 31 pages.
- Perovich, D. K.: Thin and thinner: Sea ice mass balance measurements during SHEBA, *Journal of Geophysical Research: Oceans*, 108, 2003.
- Renner, A. H. H., Gerland, S., Haas, C., Spreen, G., Beckers, J. F., Hansen, E., Nicolaus, M., and Goodwin, H.: Evidence of
555 Arctic sea ice thinning from direct observations, *Geophysical Research Letters*, 41, 5029–5036, 2014.
- Ricker, R., Hendricks, S., Helm, V., Skourup, H., and Davidson, M.: Sensitivity of CryoSat-2 Arctic sea-ice freeboard and thickness on radar-waveform interpretation, *The Cryosphere*, 8, 1607–1622, 2014.
- Ricker, R., Hendricks, S., Perovich, D. K., Helm, V., and Gerdes, R.: Impact of snow accumulation on CryoSat-2 range retrievals over Arctic sea ice: An observational approach with buoy data, *Geophysical Research Letters*, 42, 4447–4455, 2015.
- 560 Rinke, A., Maturilli, M., Graham, R. M., H., M., Handorf, D., Cohen, L., Hudson, S. R., and Moore, J. C.: Extreme cyclone events in the Arctic: Wintertime variability and trends, *Environmental Research Letters*, 12, 2017.



- Rösel, A., King, J., Doulgeris, A. P., Wagner, P. M., Johansson, A. M., and Gerland, S.: Can we extend local sea-ice measurements to satellite scale? An example from the N-ICE2015 expedition, *Annals of Glaciology*, pp. 1–10, 2017.
- Rösel, A., Itkin, P., King, J., Divine, D., Wang, C., Granskog, M. A., Krumpfen, T., and Gerland, S.: Thin sea ice, 565 thick snow and widespread negative freeboard observed during N-ICE2015 north of Svalbard, *Journal of Geophysical Research: Oceans*, 123, 2018.
- Sallila, H., Farrell, S.L., McCurry, J. and Rinne, E., 2019. Assessment of contemporary satellite sea ice thickness products for Arctic sea ice. *The Cryosphere*, 13(4), pp.1187-1213.
- Skourup, H., Farrell, S.L., Hendricks, S., Ricker, R., Armitage, T.W., Ridout, A., Andersen, O.B., Haas, C. and Baker, S., 570 2017. An Assessment of State-of-the-Art Mean Sea Surface and Geoid Models of the Arctic Ocean: Implications for Sea Ice Freeboard Retrieval. *Journal of Geophysical Research: Oceans*, 122(11), pp.8593-8613.
- Sturm, M.: Winter snow cover on the sea ice of the Arctic Ocean at the Surface Heat Budget of the Arctic Ocean (SHEBA): Temporal evolution and spatial variability, *Journal of Geophysical Research: Oceans*, 107, 2002.
- Sturm, M. and Holmgren, J.: Self-recording snow depth probe, Tech. rep., US patent number: 5,864,059., 1999.
- 575 Sturm, M., and Holmgren, J. : An automatic snow depth probe for field validation campaigns. *Water Resources Research*, 54, 9695–9701, 2018.
- Wang, C., Cheng, B., Wang, K., Gerland, S., and Pavlova, O.: Modelling snow ice and superimposed ice on landfast sea ice in Kongsfjorden, Svalbard, *Polar Research*, 34, 2015.
- Warren, S. G., Rigor, I. G., Untersteiner, N., Radionov, V. F., Bryazgin, N. N., Aleksandrov, Y. I., and Colony, R.: Snow 580 Depth on Arctic Sea Ice, *Journal of Climate*, 12, 1814–1829, 1999.
- Webster, M. A., Rigor, I. G., Nghiem, S. V., Kurtz, N. T., Farrell, S. L., Perovich, D. K., and Sturm, M.: Interdecadal changes in snow depth on Arctic sea ice, *Journal of Geophysical Research: Oceans*, 119, 5395–5406, 2014.
- Woods, C. and Caballero, R.: The Role of Moist Intrusions in Winter Arctic Warming and Sea Ice Decline, *Journal of Climate*, 29, 4473–4485, <https://doi.org/10.1175/jcli-d-15-0773.1>, 2016.
- 585 Yan, J., Alvestegui, D. G.-G., McDaniel, J. W., Li, Y., Gogineni, S., Rodriguez-Morales, F., Brozena, J., and Leuschen, C. J.: Ultrawideband FMCW Radar for Airborne Measurements of Snow Over Sea Ice and Land, *IEEE Transactions on Geoscience and Remote Sensing*, 55, 834–843, 2017.
- Zwally, H. J., Yi, D., Kwok, R., and Zhao, Y.: ICESat measurements of sea ice freeboard and estimates of sea ice thickness in the Weddell Sea, *Journal of Geophysical Research: Oceans*, 113, C02S15, 2008.

590

595



600

Appendix

Drill-hole label	Ice thickness	Snow thickness	Freeboard	Flooded
D0	1.76	0.34	0.13	no
D1	1.48	0.49	0.01	no
D2	0.78	0.30	0.02	no
D3	1.03	0.57	-0.03	no
D4	1.34	0.38	0.03	no
D5	1.65	0.83	-0.11	yes
D6	1.35	0.76	-0.09	yes
D7	1.36	0.28	0.07	no
D8	1.15	0.51	-0.03	yes
D9	1.96	0.51	0.07	no
Mean (Stddev)	1.39 (0.35)	0.50 (0.19)	0.01 (0.07)	

Table 2. Measurements acquired at 10 drill-hole sites located randomly across the 2-D survey field site. All values are given in meters.

605

610



615

Figure 10. Salinity profile and auxiliary data of an ice core, taken on 5 March 2015 within the vicinity of the 2-D survey field.

